Since January 2020 Elsevier has created a COVID-19 resource centre with free information in English and Mandarin on the novel coronavirus COVID-19. The COVID-19 resource centre is hosted on Elsevier Connect, the company's public news and information website.

Free Radical Biology and Medicine 177 (2021) 189–200

Contents lists available at ScienceDirect

Free Radical Biology and Medicine

journal homepage: www.elsevier.com/locate/freeradbiomed

FDA approved L-type channel blocker Nifedipine reduces cell death in hypoxic A549 cells through modulation of mitochondrial calcium and superoxide generation

Kuruba Manohar [a], Rishikesh Kumar Gupta [c,d], Parth Gupta [a], Debasmita Saha [b], Suman Gare [b], Rahuldeb Sarkar [e,f], Ashish Misra [a], Lopamudra Giri [b,*]

[a] Department of Biotechnology, Indian Institute of Technology, Hyderabad, 502285, India
[b] Department of Chemical Engineering, Indian Institute of Technology, Hyderabad, 502285, India
[c] International Institute of Molecular and Cell Biology in Warsaw, Warsaw, 02 109, Poland
[d] Postgraduate School of Molecular Medicine, Medical University of Warsaw, Warsaw, 02-091, Poland
[e] Departments of Respiratory Medicine and Critical Care, Medway NHS Foundation Trust, Gillingham, Kent, UK
[f] Faculty of Life Sciences, King's College London, London, UK

ARTICLE INFO

Keywords:
SARS-Cov-2
Mitochondrial calcium
Nifedipine
Hypoxia
Calcium channel blocker
Reactive oxygen species (ROS)

ABSTRACT

As hypoxia is a major driver for the pathophysiology of COVID-19, it is crucial to characterize the hypoxic response at the cellular and molecular levels. In order to augment drug repurposing with the identification of appropriate molecular targets, investigations on therapeutics preventing hypoxic cell damage is required. In this work, we propose a hypoxia model based on alveolar lung epithelial cells line using chemical inducer, $CoCl_2$ that can be used for testing calcium channel blockers (CCBs). Since recent studies suggested that CCBs may reduce the infectivity of SARS-Cov-2, we specifically select FDA approved calcium channel blocker, nifedipine for the study. First, we examined hypoxia-induced cell morphology and found a significant increase in cytosolic calcium levels, mitochondrial calcium overload as well as ROS production in hypoxic A549 cells. Secondly, we demonstrate the protective behaviour of nifedipine for cells that are already subjected to hypoxia through measurement of cell viability as well as 4D imaging of cellular morphology and nuclear condensation. Thirdly, we show that the protective effect of nifedipine is achieved through the reduction of cytosolic calcium, mitochondrial calcium, and ROS generation. Overall, we outline a framework for quantitative analysis of mitochondrial calcium and ROS using 3D imaging in laser scanning confocal microscopy and the open-source image analysis platform ImageJ. The proposed pipeline was used to visualize mitochondrial calcium and ROS level in individual cells that provide an understanding of molecular targets. Our findings suggest that the therapeutic value of nifedipine may potentially be evaluated in the context of COVID-19 therapeutic trials.

1. Introduction

Since December 2019, the COVID-19 outbreak has caused a life-threatening pandemic caused by a novel coronavirus, severe acute respiratory syndrome coronavirus 2 (SARS-CoV-2). During infection, SARS-CoV-2 multiply much faster into the body of the host and progress into severe acute respiratory distress syndrome (ARDS), associated with hypoxia [1,2]. More than 242 million are infected, and 4.93 million people are killed worldwide due to this pandemic as of Oct 22, 2021 (https://coronavirus.jhu.edu/map.html). Hypoxia is involved in various stages of COVID-19 progression [3], which damage the cells, alongside dysregulated immune response, and remains the main driver for organ dysfunction and mortality in severe COVID-19 patients [4,5]. However, due to the rapidity of the spread of the SARS-CoV-2, the rapid emergence of new variants, and loss of life during this pandemic, developing a new drug and the time taken in the process may not be practical. Hence the outbreak has demanded an urgent need for more research into the repurposing of FDA approved drugs in the protection of epithelial cells during severe infection and hypoxic conditions.

The low oxygen-induced hypoxia chambers with a CO_2 incubator with a regulated oxygen supply could be useful for studying hypoxia [5]. However, it has certain limitations, such as, while the opening of the

* Corresponding author.
E-mail address: giril@che.iith.ac.in (L. Giri).

https://doi.org/10.1016/j.freeradbiomed.2021.08.245
Received 26 June 2021; Received in revised form 26 August 2021; Accepted 29 August 2021
Available online 16 October 2021

hypoxia chamber and imaging of cell morphology, oxygen can re-enter and defuse into the hypoxia chambers. Furthermore, applying heavy machinery to study hypoxia in a laboratory setting is not possible and will not allow doing all types of experiments, including intracellular imaging [6]. Hence, in this study, we have used the other alternative of induction of hypoxia using chemical agents, $CoCl_2$. Intracellular hypoxia is known to upregulate the *HIF-1α* and p^{53} gene expression levels in A549 cells that lead to apoptosis [7–9]. Furthermore, $CoCl_2$ is known to mimic the hypoxia by upregulation of *HIF-1α* and *p53* expression in various cell lines [6,9–12]. Specifically, it has been shown that *HIF-1α* is upregulated by 1.3 fold in A549 cells with 600 μM $CoCl_2$ treatment for 24 h [13]. Other investigations also showed that a 5-9-fold increase in *HIF-1α* could be achieved at various $CoCl_2$ concentrations [9]. Since A549 cells have already been used as an experimental model to study cellular effects of SARS-CoV-2 on lung cells and expression levels of *IL-6, IL-8, NF-κB* genes [15,16], we chose the A549 cell line for investigation of hypoxic effects for the current study.

Calcium ion (Ca^{2+}) channels have emerged as key host factors for a variety of viral infections [17]. In general, calcium channel blockers (CCBs) have been shown to have antiviral activity [14], highlighting the new potential for drug repurposing. Using different cell line models (293T, Calu-3, and A549), recently, it has been reported that CCBs inhibit Ca^{2+}-mediated membrane fusion and consequently suppressed several types of COVID-19 phenotypes (infections by SARS-CoV, MERS-CoV, or SARS-CoV-2) [18]. Moreover, these CCBs are widely used for cardiovascular diseases (hypertension and angina pectoris) and therefore are safe to be used [19]. Since the injured cardiac cells are known to accumulate calcium under hypoxia, the use of nifedipine and has been shown to be cardioprotective with hypothermia as an additive [20,21]. Elevated intracellular Ca^{2+} level increases the apoptotic rate in A549 cells [22] by inducing reactive oxygen species (ROS) levels in hypoxia-induced cells [23]. ROS acts as a secondary messenger for stabilizing *HIF-1α* in hypoxia-induced A549 cells [24]. L-type calcium channels (CaV1.1 – CaV1.4) are localized on the plasma membrane, are mainly responsible for calcium entry into the cells [19]. Previously FDA-approved channel blockers, including amlodipine, nifedipine, and felodipine, have been tested to reduce SARS-CoV-2 infection, where nifedipine and amlodipine showed strong inhibition towards viral entry and infection in lung epithelial cells [25]. It has also been shown that inhibition of intracellular calcium reduces influenza A viral infection by reducing the cytosolic calcium, mitochondrial calcium, and ROS levels in A549 cells [26]. Moreover, nifedipine is known to reduce hypoxic pulmonary vasoconstriction in chronic obstructive pulmonary disease (COPD) patients [27]. Nifedipine is generally used for reducing pulmonary hypertension in certain diseases inducing high pulmonary artery pressure [28]. Previously, it has been shown that prophylactic administration of nifedipine leads to reduced inflammation in rats under hypoxia [29]. The corresponding investigation in molecular mechanism shows that nifedipine is able to suppress the upregulation of *NFkB* and stabilize the *HIF-1α* accumulation in hypoxic rats compared to control. It has also been reported that nifedipine inhibited inflammation and oxidative stress via activation of nuclear factor erythroid-2-related factor 2 (Nrf2) signaling pathway [30,31]. Once cells are subjected to oxidative stress, there is an increase in the expression of Nrf2 followed by the translocation to the nucleus [30]. Translocation of Nrf2 is known to activate the phase II detoxification enzymes and antioxidant enzyme expression through an enhancer sequence known as the antioxidant-responsive element (ARE) [30]. Also, it has been shown that the prophylactic activation of Nrf2 can be a novel therapeutic strategy under hypoxic stress [30,31]. Another drug, melatonin, mainly synthesized and secreted by the pineal gland, is known to modulate the *HIF-1α* and *VEGF* expression in $CoCl_2$ induced hypoxia in A549 cells [24]. Melatonin is also shown to have antioxidant properties through activation of Nrf2 and directly scavenging of free radicals inside the cell [32,33].

Considering the above background on CCBs, in the present work, we hypothesized that the protective effect of nifedipine in A549 cells is mediated by the reduction of sequestration of cytosolic calcium and mitochondrial calcium overload. To test our hypothesis, we performed a 3D imaging assay and examined nifedipine's ability to reduce the mitochondrial calcium overload in A549 cells and then determined whether such effect was related to the reduction of ROS and nuclear condensation. Here we present a pipeline for quantitative, multidimensional analysis of mitochondrial calcium, ROS, and nuclear condensation based on laser scanning confocal microscopy (LSCM) and the open-source image analysis platform ImageJ/Fiji. In this, we discovered a superior method for accurate identification of individual cell mitochondrial calcium and ROS levels in drug-treated lung cells. Moreover, we outline a framework for quantitative description of nuclear condensation, single-cell cellular morphology, and subsequent phase separation during apoptosis using differential interfering contrast imaging. Finally, applying this pipeline, we quantitatively distinguish cytosolic and mitochondrial calcium along with morphological changes during induction of chemical hypoxia and drug treatment, assessing the protective effect of drugs for COVID-19. Since the existing studies on nifedipine focus on pre-treatment or preconditioning with nifedipine [29,31,34–37], in this work, we aim to show the protective effect when the cells were already subjected to hypoxic stress for 24 h. Moreover, we show the cellular and molecular basis for nifedipine-mediated protection of hypoxic cells under non-prophylactic treatment conditions.

Furthermore, a high-resolution analysis using LSCM was performed to understand the specific intracellular biomarkers significantly reduced in the presence of nifedipine. One of the major contributions of this work is to demonstrate the feasibility of using 4D imaging using LSCM to visualize and quantitate the mitochondrial calcium load and ROS generation in individual cells under hypoxic stress and drug treatment. Moreover, we extend our analysis in the measurement of cytosolic calcium, phase separation features, as well as nuclear condensation. It is rather difficult to understand the details of mitochondrial states and nuclear condensation status in single cells through conventional biochemical methods and standard fluorescent microscopy. The results indicate that nifedipine can be a potential drug that can be used as a protective molecule to treat the pathophysiological condition of lungs in severe COVID-19 patients. The proposed work indicated that the protective activity was mediated by reduction of cytosolic calcium accumulation and subsequent mitigation of mitochondrial overload that mediates the nuclear condensation and apoptosis.

2. Materials and methods

2.1. Cell culture

A549 cells were purchased from National Centre for cell science Pune. Cells were cultured in a 29 mm glass-bottom cell culture dish (Cellvis, USA). Cells were cultured in DMEM medium (Hyclone, USA) supplemented with 10% fetal bovine serum and 1% pen strep (penicillin/streptomycin) (Gibco, USA) and were maintained at 37 °C in an incubator (ASTEC, Japan) with 5% CO2 and 95% air until 70–80% confluency.

2.2. Induction of $CoCl_2$ mediated hypoxia and drug treatment

Cells were seeded at 1×10^5 cells/mL in a 29 mm glass-bottom dish (1 mL) and were incubated at 37 °C with 5% CO2 and 95% air for 24 h to approximately 80% confluency. Later, cells were treated with serum-free media (Hyclone, USA) and incubated at 37 °C for 12 h. Further hypoxia was induced using 600 μM of $CoCl_2$ (Sigma Aldrich, Switzerland), and the cells were incubated at 37 °C for 24 h. After 24 h of treatment with $CoCl_2$, cells were treated with 10 μM of Nifedipine (Sigma Aldrich, China) and maintained for another 24 h in the same conditions. Apart from the drug-treated condition, control cells (without any treatment), treatment with only 600 μM $CoCl_2$, and treatment with

only 10 μM Nifedipine were maintained with the same conditions.

2.3. Cell viability assay

Cell viability was assessed using the Trypan blue (TB) (Gibco, USA) assay. Growth media was removed for cells treated with CoCl2 and nifedipine and control cells, and cells were washed with 500 μL HBSS (without calcium and magnesium) (Gibco, USA). Then we added 200 μL of Trypsin-EDTA solution (Gibco, China) to trypsinize the cells. Next, cells were resuspended in 800 μL culture media using to obtain a cell suspension. This cell suspension and 0.4% TB solution mixed in a 1:1 ratio. From this mixture, 10 μL volume was taken for the cell counting using an image-based cell-counter (Invitrogen, Singapore) to analyze the viability of the cells. Cells were seeded in glass-bottom dishes and were imaged in a phase-contrast microscope to monitor cell morphology at three different time points 48, and 72 h using 20X objective. A549 cells were seeded at a density of 1.0×10^5 on a 29 mm glass-bottom dish (498 thickness) and incubated for 24 h. After that, hypoxia was induced using 600 μM $CoCl_2$ (Sigma Aldrich, Switzerland) and incubated at 37 °C for 24 h. The concentration of $CoCl_2$ used in this study was selected such that the cells are maintained at continued hypoxic conditions before treatment with the drug. After inducing hypoxia for 24 h, cells were treated with 10 μM of Nifedipine (Sigma Aldrich, China) 500 μM melatonin (Sigma, USA) and incubated for another 24 h. Control cells (without any treatment), hypoxic cells with 600 μM $CoCl_2$ and cells with only 10 μM Nifedipine/500 μM melatonin treatment were maintained with the same conditions.

2.4. Measurement of cytosolic calcium

To monitor cytosolic calcium, cells were loaded with 5 μM Fluo-4 AM (Invitrogen, USA) at 37 °C for 20 min, followed by three times washing with 10 min intervals for each washing with HBSS. After that, Fluo-4 images were acquired in Nikon inverted microscope (Excitation: 470/40 nm; Emission: 534/55 nm).

2.5. 3D imaging of mitochondrial calcium using LSCM

To monitor the mitochondrial matrix calcium level ($[Ca^{2+}]_m$), cells were loaded with 0.2 μM cell-permeant mitochondrial specific fluorescent Ca^{2+} indicator Rhod-2 AM dye (Invitrogen, USA) at 4 °C for 1 h, followed by incubation at 37 °C for 30 min as previously described [38]. The Rhod-2 imaging was performed with an excitation wavelength of 561 nm, and 3D imaging of cells was performed consisting of 120 stacks that span 5 μm using a 63X oil objective. To analyze $[Ca^{2+}]_m$ level, we performed a 2D compression of all z-stacks in 5 μm, and regions of interest (n = 10) were drawn manually in the 30 cells corresponding to each treatment (quantification of mitochondrial calcium accumulation). Further, the average Rhod-2 fluorescence intensity in each cell was quantified using LASX software. Rhod-2 staining and imaging were performed to monitor mitochondrial Ca2+ for control cells, nifedipine treated cells, CoCl2 treated cells, and CoCl2 treated cells, followed by nifedipine treatment.

2.6. Imaging hypoxia-induced ROS formation

During hypoxia exposure, as mentioned in the above experiments, cells were treated with Nifedipine and melatonin, and Intracellular ROS were detected using MitoSOX dye (Invitrogen, USA). In addition, 3D imaging was performed using LSCM (Leica, Germany) at excitation at 561 nm using 63X oil objective. 120 z-stacks were obtained in a span of 5 μm and were merged to obtain a 2D image. The region of interest (n = 10) in each cell was drawn manually, and the average intensity per cell was obtained in a pseudo-color scale from 0 to 255 units using LASX software.

2.7. Live-cell imaging Hoechst staining

For Hoechst 33342 (Invitrogen, USA) staining, 2 mL 50 μM Hoechst 33342 staining (Sigma Aldrich, USA) was used for 30 min at 37 °C. Then cells were washed three times with 1X–PBS (Gibco, USA) and were immediately imaged with the 63X oil objective in the confocal microscope. Live imaging of the nucleus was performed using 3D imaging, and 50 z-stacks in a span of 25 μm were collected to obtain the distribution of Hoechst intensity along z-direction in each cell.

2.8. Quantification of mitochondrial calcium (Rhod-2) and ROS generation (MitoSOX) using 3D reconstruction and 2D compression

Multiple z-stacks corresponding to different focal planes were scanned to construct 3D images within the cell. Rhod-2 and MitoSOX intensity was captured by photomultiplier tube (PMT) scanning for a total of 120 stacks (designated as one complete z-scan), which corresponds to a thin disk-like section of thickness 5 μm. In order to obtain the spatial distribution of mitochondrial calcium and ROS generation, a 3D reconstruction was obtained from the z-stacks using LASX software. To account for the Rhod-2 intensity from all z-stacks, individual stack images were first merged using LASX software. Then we obtained compressed z-stack images (2D merged image) version through the superimposition of all the z-stacks, corresponding to each condition Average Rhod-2 and MitoSOX intensities were evaluated from manually chosen regions of interest (ROIs). To obtain Rhod-2 and MitoSOX intensities corresponding to these ROIs, intensities from individual focal planes were summed across the entire sample thicknesses to obtain $F_{measured} = F1 + F2 + \ldots Fn$, where Fi represents fluorescence intensity for the ROI obtained from each z-stack. The complete workflow for 3D imaging, reconstruction, and compression in 2D is depicted in Supplementary Fig. 1. Table S1 shows the 3D imaging parameters for measuring the intensity of Rhod-2, Hoechst, and MitoSOX in single cells.

2.9. Immunocytochemistry assay

A549 cells were seeded at a density of 1×10^5 cells/coverslip and incubated for 24 h. Further, hypoxia was induced using 600 μM $CoCl_2$ (Sigma Aldrich, Switzerland) and incubated at 37 °C for 24 h. After inducing hypoxia for 24 h, cells were treated with 10 μM Nifedipine (Sigma Aldrich, China). Control cells (without any treatment) and hypoxic cells with 600 μM $CoCl_2$ were also maintained at similar conditions. Cells were fixed with 4% paraformaldehyde in phosphate-buffered saline (PBS) (pH, 7.4) at room temperature for 20 min. The cells were then washed three times with PBS and permeabilized with 0.5% Triton X-100 for 15 min. After that, cells were blocked with 2% BSA (Sigma-Aldrich) diluted in PBS for 2 h at room temperature. The cells were incubated anti-Nrf2 human polyclonal primary antibody (1:300, Santa Cruz Biotechnology, Dallas, TX, USA) for 12 h at 4 °C. After that, cells were washed three times with PBS and then incubated with a secondary antibody (Alexa Fluor 594-conjugated anti-rabbit antibody, 1:600 dilutions, Life technologies) for 2 h at 4 °C. Afterward, the cells were washed two times with PBS and stained with Hoechst for 10 min at room temperature. The images were acquired with a laser scanning confocal microscope fluorescence microscope (Leica TCS SP8, USA).

2.10. Quantitative real-time reverse transcription (qRT-PCR)

Total RNA was extracted from A549 cells using TRIzol reagent following the manufacturer's protocol. cDNA was synthesized from total RNA using Superscript II.

Reverse Transcriptase (Invitrogen, USA) according to manufacturer's protocol. qRT-PCR was done using Fast SYBR TM Green Master Mix (Applied Biosystems, USA), with the following primers: Nrf2 (forward, 5′-CAGCGACGGAAAGAGTATGA-3'; reverse, 5′-

TGGGCAACCTGGGAGTAG-3′), β-actin (forward, 5′-CTGGAACGGTGAAGGTGACA-3’; reverse, 5′-AAGGGACTTCCTGTAACAATGCA-3′). All fluorescent qRT-PCR assays were performed in triplicate 20-μL reactions, and detection was carried out using a QuantStudio 1 Real-time PCR System (Applied Biosystems, USA). The thermocycling conditions were: 95 °C for 20 s, 40 cycles of amplification (95 °C for 1 s and 60 °C for 20 s), 95 °C for 1 sec, 60 °C for 20 s and 95 °C for 1 s. The gene expression levels for each amplicon were calculated using the ΔΔCT method [39] and normalized against β-actin mRNA. The difference in expression between the control and experimental groups was calculated as 2-ΔΔCT.

2.11. Statistical analysis

All experiments were repeated at least three times, and representative results are shown. The differences between the two treatment groups were compared with a *t-test* and Kruskal-Wallis test (MATLAB). A two-tailed $P < 0.05$ was considered to indicate statistical significance. Data are presented as the mean ± standard deviation (SD).

3. Results

3.1. Protective effect of nifedipine in A549 cells under hypoxic condition

In order to evaluate the $CoCl_2$ mediated toxicity during induction of chemical hypoxia in A549 cells, we first performed the measurement of cell viability using 400 μM and 600 μM of $CoCl_2$. Supplementary Fig. 2 shows that the number of cells having aberrant morphology were higher in the case of 600 μM $CoCl_2$ treatment for 48 h compared to 400 μM $CoCl_2$ treatment. Next, we performed dose-dependent toxicity analysis for A549 cells using a treatment of 1, 5, 10, and 15 μM nifedipine (Supplementary Fig. 3a). The result shows that the cell viability is maintained within 75–83% when treated with 1, 5, and 10 μM nifedipine. Additionally, we performed a dose-dependent protectivity assay using 1, 5, 10, and 15 μM nifedipine treatment for the $CoCl_2$ treated hypoxic A549 cells. The result shows that 10 μM nifedipine yields maximum viability and significant recovery in morphology for $CoCl_2$ treated cells (Supplementary Figs. 3b, c, and d). It was observed that 10 μM nifedipine provides optimal protection against $CoCl_2$-induced cell death, similar to previous studies on nifedipine treatment in human chondrocytes [55].

Hereafter, in order to assess the protective effect of nifedipine under a higher level of hypoxic stress, we selected 600 μM of $CoCl_2$ and 48 h as the treatment time for induction of chemical hypoxia in A549 cells. After 24 h of 600 μM $CoCl_2$ addition, the cells were treated with 10 μM Nifedipine for 24 h, followed by cell morphology and cell viability measurement. In this experiment, we checked if nifedipine, an L-type calcium channel blocker, has a protective effect on cells treated with $CoCl_2$ (Fig. 1a). Fig. 1b shows that cell viability was significantly lower for 24 h of 600 μM $CoCl_2$ treatment compared to the viability of the cells

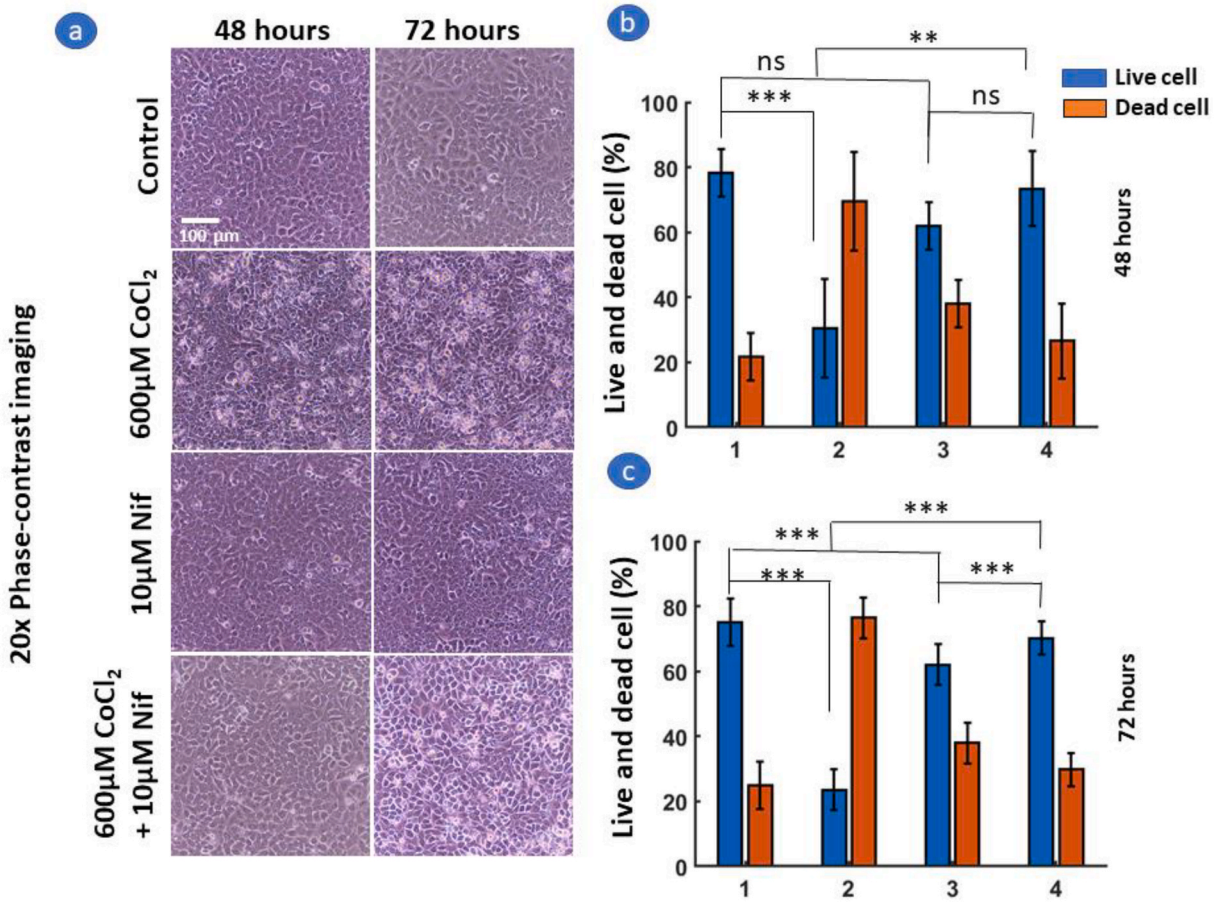

Fig. 1. Nifedipine shows a protective effect for $CoCl_2$ treated A549 cells. a) Phase contrast images after treatment with $CoCl_2$ at 48 and 72 h. Excess dead cells were observed in 600 μM $CoCl_2$ treatment. b) and c) Percentage of live cells (Blue) and dead cells (orange) in A549 cells after various combination of treatment (1-control, 2–600 μM $CoCl_2$, 3–10 μM Nifedipine and 4–600 μM $CoCl_2$ + 10 μM Nifedipine). Cell viability was measured using Trypan blue assay at 48 and 72 h and was represented in the bar diagram. Data are indicated as mean ± SD (n = 20). $P < 0.05$(*), $p < 0.01$(**), and $p < 0.001$(***) and $p > 0.5$ (ns-no significance), Kruskal-Wallis test. Here the time points are mentioned with respect to $CoCl_2$ treatment. (For interpretation of the references to color in this figure legend, the reader is referred to the Web version of this article.)

without $CoCl_2$. However, there was a significant increase in cell viability in the cells which were treated with 10 μM Nifedipine after 24 h of treatment of 600 μM of $CoCl_2$ (Fig. 1a and b). The result clearly shows that nifedipine has a protective effect on cells treated with $CoCl_2$ upto 48 h (Fig. 1c).

3.2. Nifedipine retains the cell shape and integrity

Cell death under hypoxic stress was generally characterized by cell shrinkage, nuclear fragmentation, and membrane blebbing [40]. Also, the stressed condition leads to phase separation followed by stress granule formation inside cells. In order to investigate the restoration of phase separation and cell shape with the treatment of nifedipine, we performed time-lapse monitoring using confocal brightfield (BF) imaging for 1 h. Fig. 2 shows the comparison of the single representative cell from $CoCl_2$ induced hypoxic condition and condition with nifedipine treatment. Fig. 2b shows that $CoCl_2$ induced-hypoxic cells undergo a change in morphology and cell shrinkage leading to cell death. Fig. 2d shows that the cell shape and morphology are restored in hypoxic cells, which are treated with nifedipine. Moreover, time-lapse images indicate separation of phases, forming cell blebbing in $CoCl_2$ treated condition (Fig. 2b). The time-lapse imaging of cells treated with nifedipine shows that nifedipine helps in retaining cell shape and inhibit the gradual process of phase separation observed in hypoxic condition (Fig. 2d). In control cells and nifedipine-treated cells, no significant change in cell morphology was observed (Fig. 2a, c). Supplementary Fig. 4 shows that the number of cell death was higher in the case of $CoCl_2$ treated condition compared to treatment with $CoCl_2$ + nifedipine. Supplementary Video 1 shows the dynamics of cell shrinkage, formation of membrane blebs, and movement of cells for CoCl2 treated condition in a 1-h time scale. Overall, the results clearly show that nifedipine was helping in retaining the cell shape under stressed conditions (Supplementary Video 2).

3.3. Nifedipine mediated modulation of cytosolic calcium and mitochondrial calcium overload

Since nifedipine is an L-type calcium channel blocker, we further hypothesize that this drug will reduce the calcium accumulation associated with hypoxic stress. Also, mitochondrial Ca^{2+} overload can induce mitochondrial ROS production. Hence, we further investigated if nifedipine reduces the cytosolic calcium and subsequently mitochondrial Ca^{2+} overload in the $CoCl_2$ treated A549 cells [41]. In order to examine the mitochondrial Ca^{2+} in the hypoxia-induced cells, we performed 3D imaging using Rhod-2 dye. Fig. 3 shows the Fluo-4 intensity in cells under various treatment conditions, whereas Fig. 4 shows the Rhod-2 intensity in representative cells for the same treatment conditions. Fluorescent imaging of A549 cells stained with Fluo-4 dye and Rhod-2 dye exhibited a higher level of cytosolic calcium, sequestration of calcium in the smaller domain, and overload of mitochondrial Ca^{2+} stress in the $CoCl_2$ treated single cell as shown in Figs. 3b and 4b. Supplementary Fig. 5 shows the x-z view of 3D-reconstruction of Rhod-2 staining in cell population for four conditions, and the results indicate that the mitochondrial overload is less in cells treated with $CoCl_2$ and nifedipine compared to cells treated with only $CoCl_2$. Such sequestration of cytosolic calcium and subsequent mitochondrial Ca^{2+} overload was not observed in control cells as well as nifedipine-treated A549 cells presented in Fig. 3a, c, and Fig. 4a, c, respectively. The results clearly indicate that treatment with nifedipine after induction of hypoxia significantly reduces the accumulation of cytosolic calcium (Fig. 3d and e). Sequestration of calcium in granular structure and mitochondrial Ca^{2+} load is significantly lower in the case of nifedipine treatment compared to $CoCl_2$ treated cells (Fig. 4d and e). Fig. 3e also shows no significant difference between cytosolic calcium levels between treatment with nifedipine and treatment with $CoCl_2$ + nifedipine.

In order to examine the dynamics of mitochondrial Ca^{2+} in $CoCl_2$ treated cells, we also performed time-lapse imaging for the 1 h in $CoCl_2$

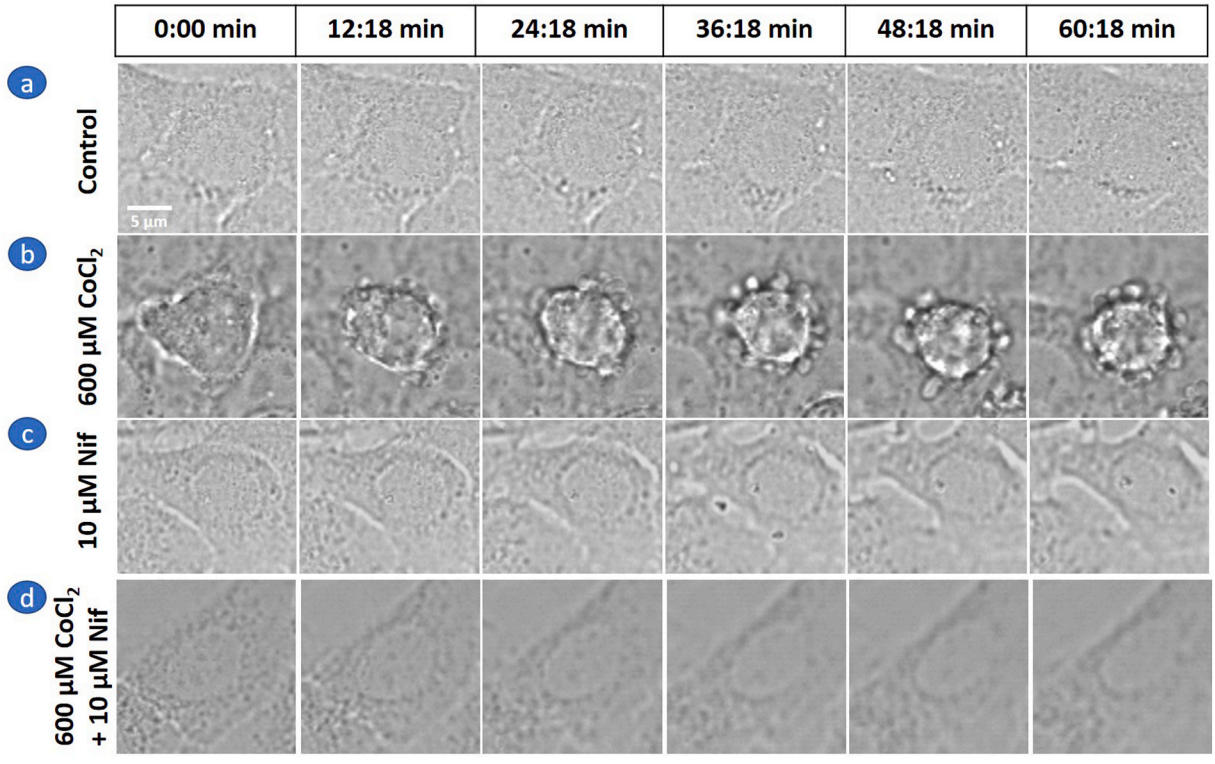

Fig. 2. Time-lapse imaging of cell morphology during treatment with $CoCl_2$ and a typical revival with nifedipine (1-h time frame). Representative images of single-cell morphology were captured by confocal brightfield imaging in various combinations of treatments a) control, b) 600 μM $CoCl_2$, c) 10 μM Nifedipine, and d) 600 μM $CoCl_2$ + 10 μM Nifedipine. A549 cells were treated with $CoCl_2$ for 24 h, followed by treatment with nifedipine for 24 h. Nif- Nifedipine, 63X oil objective was used for imaging.

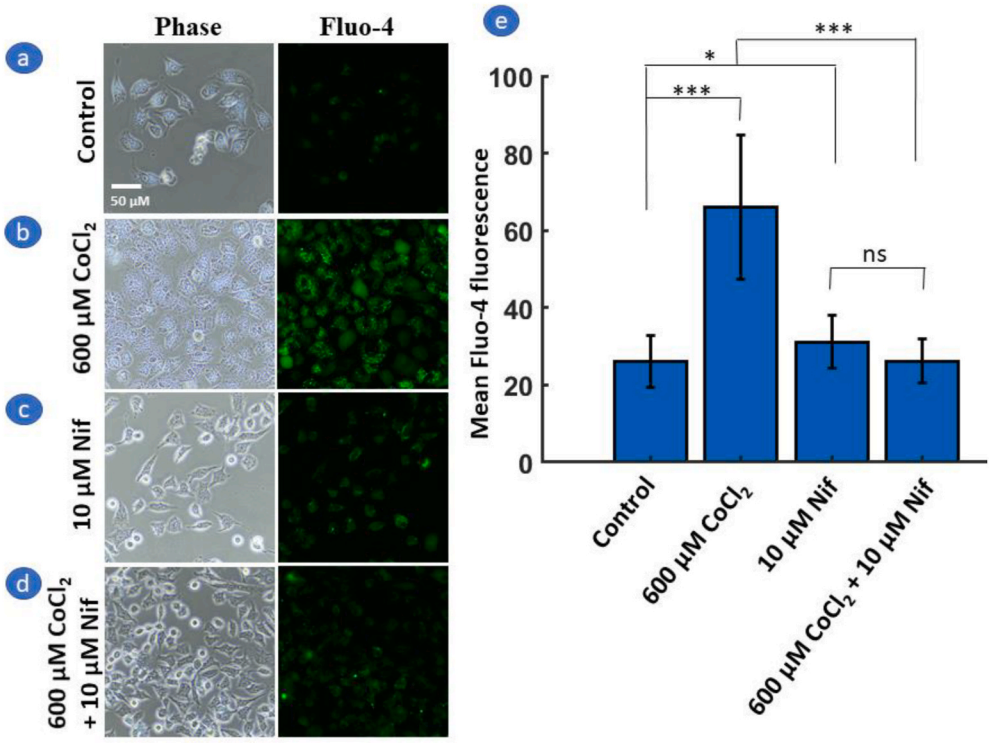

Fig. 3. Nifedipine treatment leads to a reduction in the accumulation of cytosolic Ca^{2+} in A549 cells treated with $CoCl_2$. a) Representative phase-contrast images (40x objective) and fluorescent images of Fluo-4 intensity (2nd column) for various combinations of treatments. a) Control, b) 600 µM $CoCl_2$, c) 10 µM Nifedipine and d) 600 µM $CoCl_2$ + 10 µM Nifedipine. e) Bar graph representing the average Fluo-4 mean intensity values for each condition shows the effect of nifedipine on cytosolic Ca^{2+} level. Data are indicated as mean ± SD (n-15 cells). $p < 0.05$(*), $p < 0.01$(**), and $p < 0.001$(***) and $p > 0.5$ (ns-no significance), Kruskal-Wallis test. Images 40X objective.

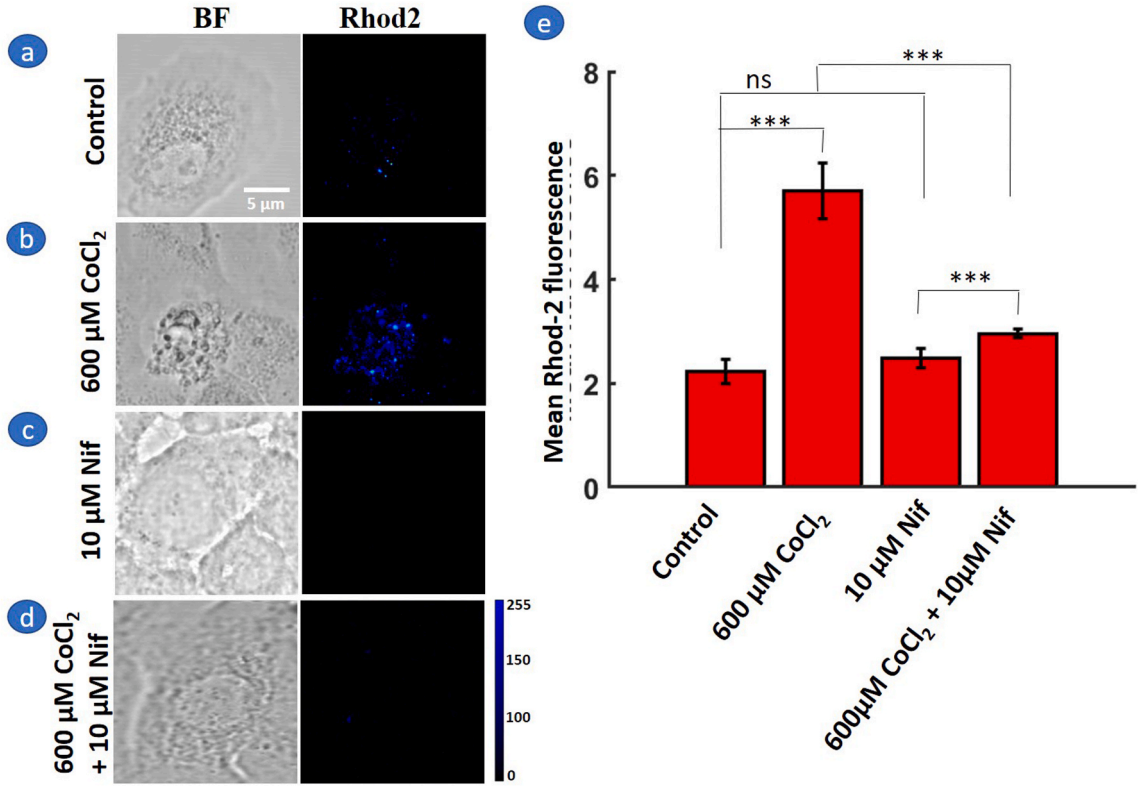

Fig. 4. Nifedipine treatment leads to a reduction in mitochondrial Ca^{2+} in A549 cells treated with $CoCl_2$. Representative brightfield images (63×-oil objective) of single-cell (first column) and heat map representation of Rhod2 distribution from 2D compression (second column) for various combination of treatments a) control, b) 600 µM $CoCl_2$, c) 10 µM Nifedipine and d) 600 µM $CoCl_2$ + 10 µM Nifedipine. e) Bar graph representing the mean Rhod-2 mean intensity values for each condition shows the effect of nifedipine on mitochondrial Ca^{2+} level. Data are indicated as mean ± SD (n-30 cells). $p < 0.05$(*), $p < 0.01$(**), and $p < 0.001$(***) and $p > 0.5$ (ns-no significance), Kruskal-Wallis test. Images were acquired using a 63X oil objective.

treated cells. Supplementary Video 3 shows that $CoCl_2$ treated cells having a higher level of mitochondrial Ca^{2+} overload (at 0:00 min) compared with the other conditions. Interestingly, we noticed another phenomenon that the cells which were in the apoptotic death process were losing the adherence from the bottom of the dish (decrease in Rhod-2 stain within the height of imaging plane, 5 μm). On the other hand, Supplementary Video 4 shows that the nifedipine-treated hypoxic cells show minimal mitochondrial Ca^{2+} overload compared to $CoCl_2$ treated cells. Overall, the results showed that nifedipine facilitates the protective effect by modulating cytosolic calcium and mitochondrial calcium overload.

3.4. Nifedipine reduced ROS generation in hypoxia-induced A549 cells

ROS-mediated oxidative stress is regarded as a potential common mediator of cell death [32]. In order to examine the ROS level in $CoCl_2$ treated cells and whether nifedipine was able to reduce the ROS levels in the A549 cells, we performed MitoSOX staining to measure the ROS levels in different conditions. Fig. 5 shows the fluorescence intensity of MitoSOX in single representative cells from each treatment condition. An increase of MitoSOX fluorescence was noticed in $CoCl_2$ treated cells indicating upregulation of intracellular ROS levels in $CoCl_2$ in A549 cells. Supplementary Fig. 6b shows that the number of cells having a higher level of ROS generation is higher in $CoCl_2$ treated cells compared to cells treated with $CoCl_2$ + nifedipine treated cells (Supplementary Figs. 6b and d). Fig. 5e shows the comparison of ROS levels in a cell population obtained from various treatment conditions. The MitoSOX fluorescence intensity for $CoCl_2$ treated cells was significantly higher than the control condition (Fig. 5e). The quantification results showed significant ROS generation reduction in 10 μM nifedipine-treated hypoxic A549 cells. However, ROS level in nifedipine-treated control cells is higher than that of 10 μM nifedipine-treated hypoxic cells ($p < 0.05$, Fig. 5e), nifedipine was able to arrest ROS generation and nuclear condensation under hypoxia. Since nifedipine treatment is known to activate the Nrf2 signaling pathway in oxidative stress by localization of Nrf2 in the nucleus [30], we further investigated the expression of *Nrf2* before and after treatment with nifedipine in $CoCl_2$ treated hypoxic cells. The qRT-PCR result shows that there is a more than 2-fold increase in the *Nrf2* expression (Fig. 5f). Also, it is observed that the higher level of *Nrf2* expression is maintained at 12 and 24 h starting from 6 h post-treatment with nifedipine. Additionally, from immunocytochemistry assay, localization of *Nrf2* was observed in $CoCl_2$ + nifedipine treated cells between 6 and 12 h (Fig. 5g).

3.5. Nuclear morphology changes in hypoxia-induced A549 cells

Since nuclear condensation and nuclear fragmentation are known to be the main features of the cell death process, we further investigated the effect of nifedipine on nuclear integrity. In order to examine the nuclear integrity under $CoCl_2$ treated condition A549 cells and whether nifedipine was restoring the nuclear integrity, we performed the time-lapse imaging using Hoechst-33342 staining for 1 h for the above mentioned four cases of treatments (Fig. 6). Fig. 6b shows that $CoCl_2$ treated cells had more nuclear condensation cells than other conditions . Although the nucleus was globular in shape in healthy cells, nuclear condensation and shape were changing dynamically with time progression. However, this phenomenon was not observed in control, nifedipine-treated, and hypoxic-nifedipine-treated cells as well (Fig. 6a, c, d). Supplementary Fig. 7 shows the progressive change in nuclear condensation under various conditions. Time-lapse images for 1 h show that $CoCl_2$ treated cells undergo nuclear condensation with time (Fig. 6b). In contrast, the nifedipine treated hypoxic cells effect does not show much change in nuclear morphology (Supplementary Fig. 7d). In order to investigate the nuclear shape in live and dead cells, we used the 3D imaging data from Hoechst-33342 stained cells and qualified intensity along the z-plane. The sixth column (3D Hoechst) of Fig. 6 shows that live cells have high intensity of Hoechst stain in the middle of the nucleus, and dead cells have distributed intensity throughout the z-plane. These results indicate that nifedipine has a protective effect on nuclear condensation, which is generally enhanced with the treatment of $CoCl_2$ and has a protective effect on $CoCl_2$ induced cell death. Supplementary Video 1 shows that $CoCl_2$ treated cells contain a higher percentage of dead cells, formation of cell blebs and apoptotic bodies, high cell movement. Moreover, these processes are associated with gradual progression in nuclear condensation and loss of integrity within a span of 1 h. In contrast, Supplementary Videos 5 and 6 show that control cells and nifedipine-treated control cells maintain cell morphology and cell nuclear integrity. Similarly, Supplementary Video 2 shows $CoCl_2$ treatment followed by nifedipine addition leads to lowering the percentage of dead cells and lesser cell movement compared to $CoCl_2$ treated cells. Also, from these visualizations and dynamic processes, it can be concluded that nifedipine helps in retaining the cell morphology and nuclear integrity.

Fig. 7a shows the details of the molecular pathway with $CoCl_2$ treatment and the progression of mitochondrial Ca^{2+} stress leading to cell death. Here, the pathway proposed here consists of L-type calcium channel blocking, subsequent reduction of mitochondrial Ca^{2+} stress, and ROS generation (Fig. 7b). This further leads to a reduction in nuclear condensation and retains cell shape and morphology. Since nifedipine has the potential to reduce most of the biomarkers for apoptosis, further optimization on nifedipine in preclinical trials can be tested for regaining integrity in epithelial cells under hypoxic conditions.

3.6. Comparison of nifedipine and melatonin in the reduction of ROS generation in hypoxia-induced A549 cells

Since melatonin is known as a drug that is known to inhibit the ROS generation in the stressed epithelial cells [42], we compared the action of nifedipine and melatonin. To compare the ROS levels inhibition in the case of $CoCl_2$ treated A549 cells with the melatonin and nifedipine, we performed MitoSOX staining (Supplementary Fig. 8). A549 cells were treated with 600 μM $CoCl_2$ for 24 h and treated with 10 μM nifedipine or 0.5 mM melatonin. Both drugs indicated a reduction in the ROS generation, and there is no significant difference in ROS level between the two drugs.

4. Discussion

In this study, we show that nifedipine treated hypoxic lung epithelial cells show reduced cell death, cytosolic calcium, mitochondrial calcium overload, ROS formation, and DNA condensation compared to the control condition. Such specific visualization of mitochondrial health using 3D imaging and time-lapse imaging of various treatment conditions have not been investigated in detail previously. One of the major novelties of this work is the evaluation of hypoxic conditions and treatment with nifedipine using live imaging.

It has been reported that severe COVID-19 patients with acute respiratory distress syndrome (ARDS) are primarily affected by hypoxemia, which is also associated with dysregulated immune response [1]. Severe hypoxemia results from pneumonia with bilateral interstitial infiltrate and vascular involvement, leading to ventilation-perfusion ratio mismatch [43]. In the cells infected with SARS-CoV-2, the hypoxia-inducible factor-1α level is elevated, reducing epithelial cell survival [44]. COVID-19 induced hypoxia occurs in lung epithelial cells associated with mucus adherence and accumulation in the alveoli, leading to the increased thickness of the blood-gas barrier and impairment of O_2 and CO_2 exchange in lung cells [45,46]. Such hypoxia-induced cells lead to an increase in cell death and organ dysfunction.

Following the need for assessing drugs that can be used to protect lung cells at certain phases of SARS-CoV-2 progression, our study focuses on repurposing FDA-approved calcium channel blocker nifedipine

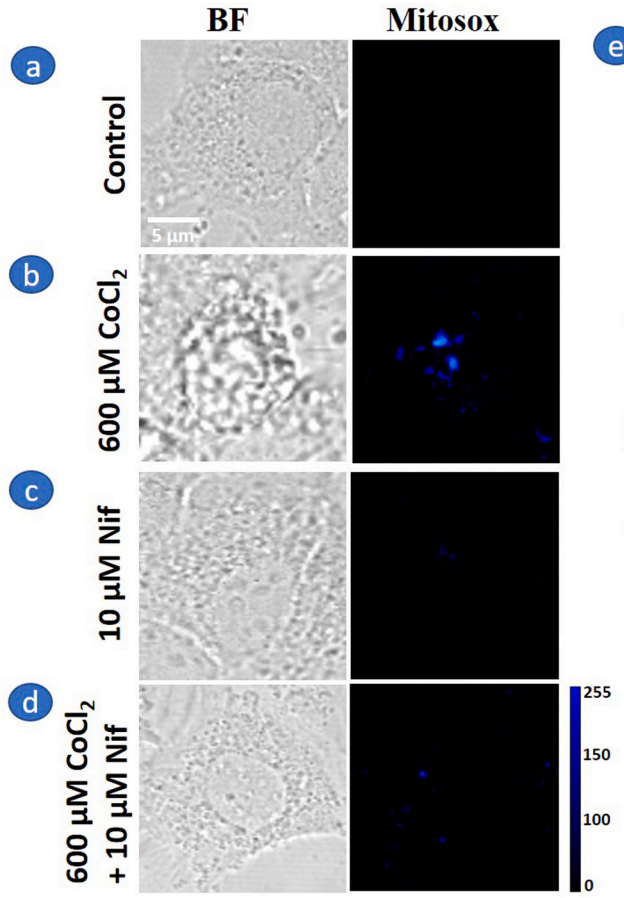

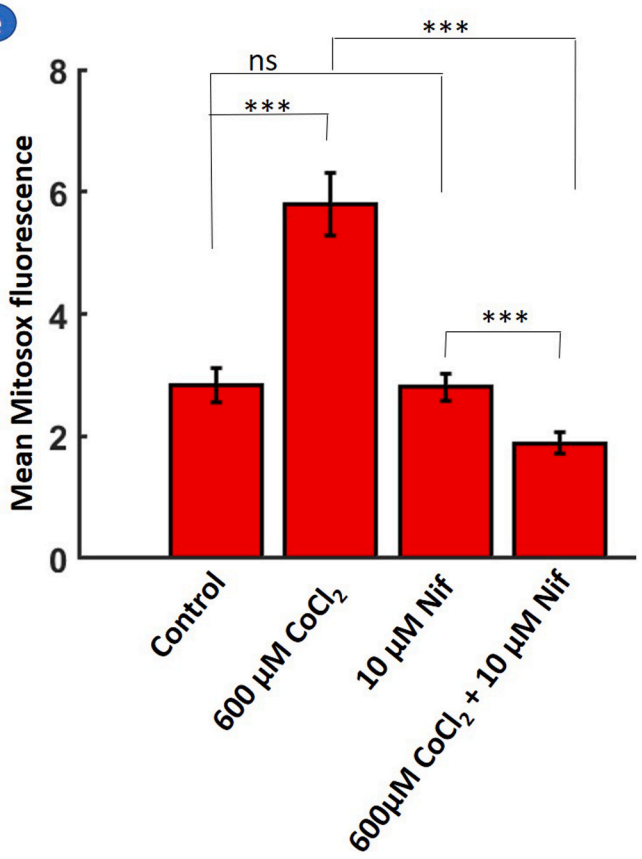

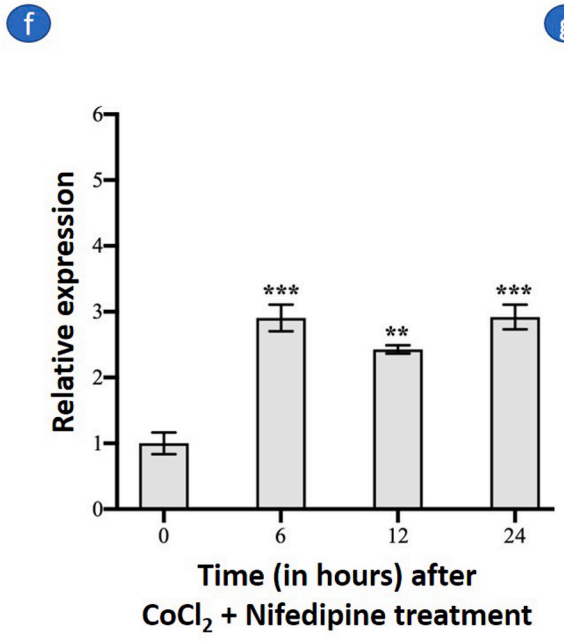

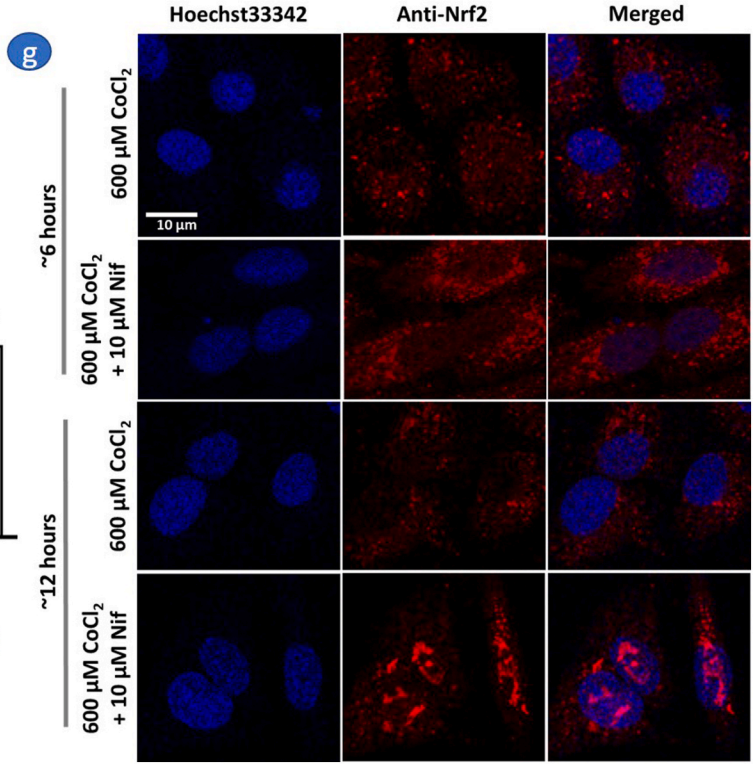

(caption on next page)

Fig. 5. Nifedipine treatment leads to a reduction in reactive oxygen species in A549 cells treated with $CoCl_2$. Brightfield - cell morphology (first column) and heat map representation of MitoSOX staining from 2D compression (second column) for various combinations of treatments (a) control (b) 600 μM $CoCl_2$, an enhanced MitoSOX fluorescence was found in 600 μM $CoCl_2$ treated A549 cells (c) 10 μM Nifedipine, treatment with nifedipine does not induce ROS, and (d) 600 μM $CoCl_2$ + 10 μM Nifedipine, (e) Bar graph representing the average MitoSOX intensity values for each condition. $CoCl_2$ induced ROS production was significantly reduced through treatment with nifedipine. Data are indicated as mean ± SD (n-30 cells). $p < 0.05$(*), $p < 0.01$(**), and $p < 0.001$(***) and $p > 0.5$ (ns-no significance), Kruskal-Wallis test. Images 63X oil objective. (f) The *Nrf2* mRNA expression levels were analyzed using qRT-PCR. $p < 0.01$(**), and $p < 0.001$(***) (g) Representative immunocytochemical labeling of *Nrf2* in A549 cells treated with 600 μM $CoCl_2$ and 600 μM $CoCl_2$ + 10 μM Nifedipine. Confocal microscopy analysis depicts nuclear localization f *Nrf2* with 600 μM $CoCl_2$ + 10 μM Nifedipine at 6 and 12 h. *Nrf2*-Red, Hoechst 33342- blue. (For interpretation of the references to color in this figure legend, the reader is referred to the Web version of this article.)

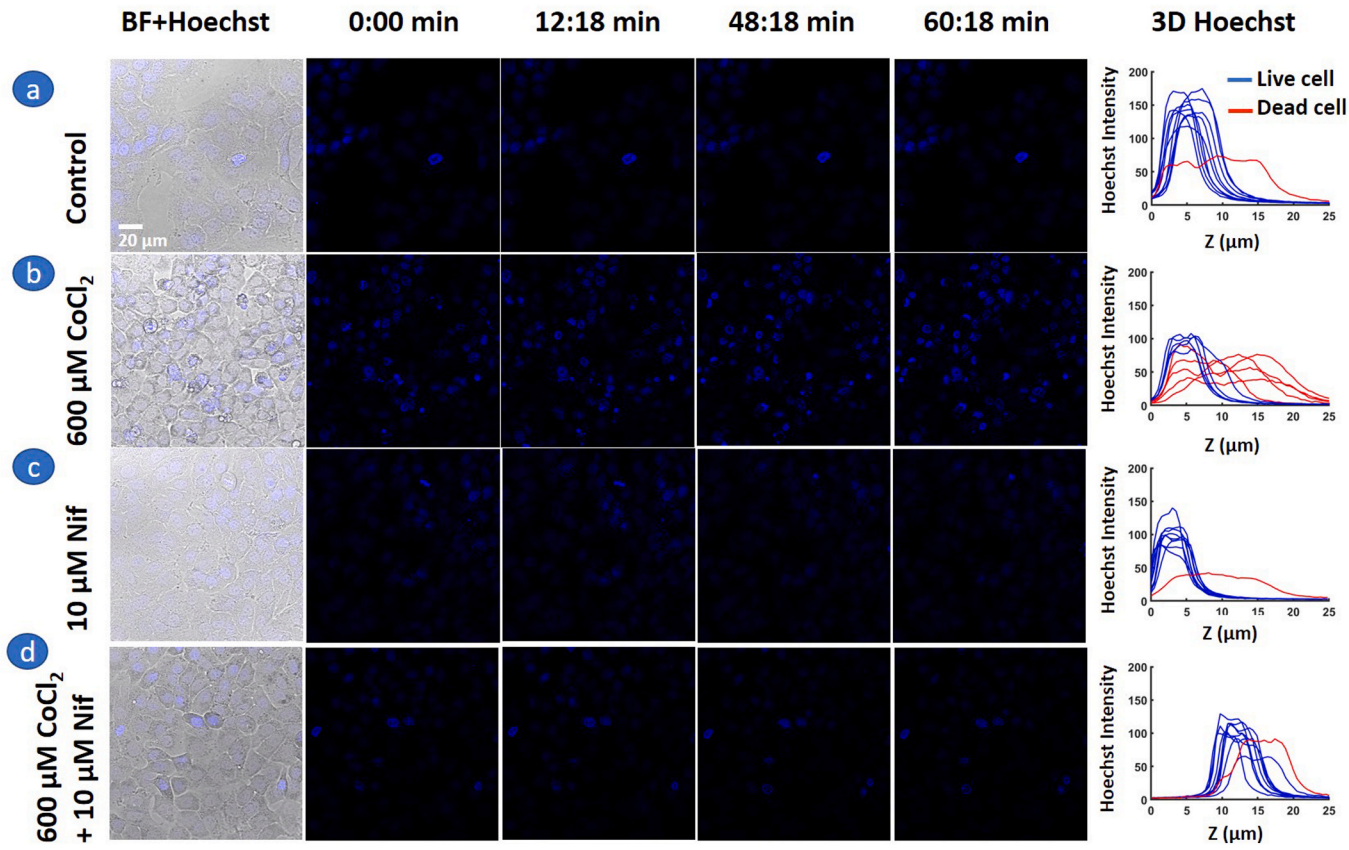

Fig. 6. Monitoring of DNA condensation during $CoCl_2$ induced cell death and nifedipine treatment using time-lapse imaging. Representative overlap images of Brightfiled -cell morphology + Hoechst 33342 staining (first column) + and time-lapse images of Hoechst 33342 (2nd, 3rd, 4th and 5th column) in A549 cells for various combination treatments. a) Control, b) 600 μM $CoCl_2$, c) 10 μM Nifedipine and d) 600 μM $CoCl_2$ + 10 μM Nifedipine. The graph in the 6th column shows mean intensity measured along the z-axis using 3D imaging (the thickness of Z stack = 25 μm) for cells with spread shape (blue) and round cells (red). Images were acquired by 63X oil objective. (For interpretation of the references to color in this figure legend, the reader is referred to the Web version of this article.)

that protects cells from hypoxia-induced cell death. Specifically, this study assumes further importance since nifedipine was found to inhibit the SARS-CoV-2 infectivity in Calu-3 and Vero cell culture. Fig. 1b and c, and Fig. 5e show that the treatment of control cells with nifedipine may induce an increase in ROS generation and induce some cell death. Also, the result shows that the cell death is more at 72 h compared to 48 h. However, further studies in tuning the dose of nifedipine and controlled release of nifedipine through nebulizer may solve the problem. More importantly, among FDA-approved calcium channel blocker drugs (CCBs), 10 μM nifedipine shows minimal cytotoxicity and higher viability of epithelial cells [25]. Also, previous studies have shown that virus (SARS-CoV and MERS-CoV) entry into the cells requires Ca^{2+} ions coordinated by amino acids present in the spike (S) proteins [44,47]. Lowering the availability of Ca^{2+} ions showed the complete reduction of SARS-CoV entry to cells, and the sequence of SARS-CoV and SARS-CoV-2 fusion proteins were identical. Thus, it suggests that SARS-CoV-2 entry into the cells is dependent on Ca^{2+} ion level [48]. In another study on mountain sickness, it has been shown that treatment with nifedipine *in vitro* prevents hypoxia cell death through activation of the *Nrf2* signaling pathway followed by translocation of Nrf2 in the nucleus [30]. In this work, we show that 10 μM nifedipine induces a significant increase in the expression of *Nrf2*. A similar increase in *Nrf2* expression and Nrf2 translocation is observed in A549 cells with redox-active pyocyanin [49]. These findings have a potential impact on reducing cell damage in various tissues resulting from hypoxemia. Under normal conditions, Nrf2 has a half-life of only 20 min [50], and in case of oxidative stress, Nrf2 translocate into the nucleus, where it binds to a DNA promoter and initiates transcription of antioxidative genes and their proteins [51]. In the future, we plan to perform the time-course analysis of Nrf2 translocation followed by *HO-1, NQO-1, SOD2* expression to identify the onset of antioxidant activity. Similarly, melatonin is also known to inhibit oxidative stress via Nrf2/HO-1 signaling pathway [33].

Dihydropyridine group of CCBs nifedipine and amlodipine are also known to be used for the treatment of hypertension and various disorders with pulmonary vasoconstriction. Severe COVID-19 patients had vasoconstrictive, pro-inflammatory, and pro-oxidative effects in lung

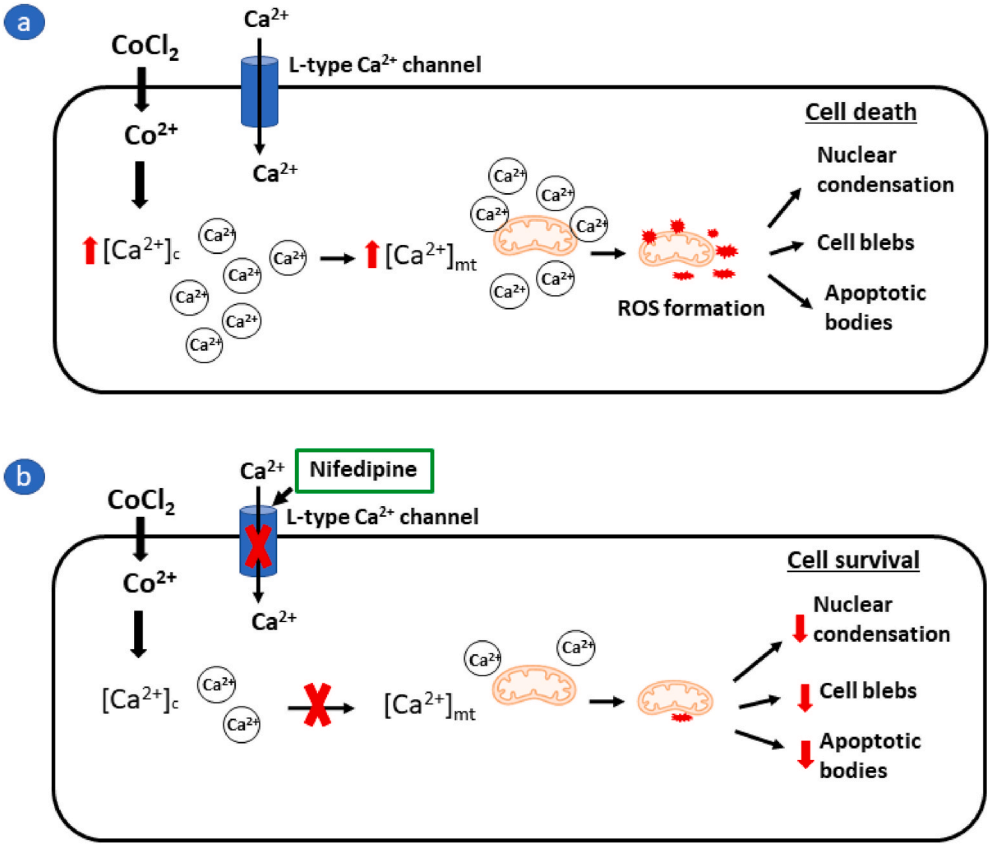

Fig. 7. Schematic diagram of the molecular pathway for the proposed mechanism a) $CoCl_2$ induces an increase in cytosolic calcium accumulation and mitochondrial calcium overload that lead to the generation of ROS b) Reduction in cytosolic calcium, mitochondrial calcium overload by nifedipine. Nifedipine is able to significantly reduce mitochondrial calcium and ROS formation by blocking L-type calcium channels.

cells [52]. As nifedipine is known to reduce pulmonary vasoconstriction in general [28], it is speculated that nifedipine may also inhibit hypoxic pulmonary vasoconstriction during COVID-19.

Since there is limited information on cellular level protection on cell morphology, cell viability, mitochondrial calcium stress, and ROS levels in hypoxic cells, we present a hypoxia model based on alveolar lung cancer cells (A549) cells using treatment with $CoCl_2$ to that can be used for testing the protection by nifedipine. The effects of drugs on mitochondria were investigated by 3D imaging using a laser scanning confocal microscope. Moreover, live imaging was used for monitoring the cell morphology at the single-cell level after treatment with the drug. However, further experiments need to be performed to obtain similar results with chamber-based hypoxia, where the effect of reoxygenation can be compared with the protective effect of nifedipine.

In this work, we used a minimal concentration of Rhod-2 (0.2 μM) to image the mitochondrial calcium overload in cells subjected to chemical hypoxia so that the effect of the dye on cell health is minimum (Supplementary Fig. 9). With these experiments, we identified the stressed cells after 24 h of hypoxic treatment in a cell population. One of the future works is to monitor the HIF1-α in these cells over the course of 48 h of $CoCl_2$ treatment and correlate the results with mitochondrial overload and ROS generation. In addition, with 3D imaging of nuclear staining (Hoechst 33342), it was deciphered that the healthy cells have a globular nucleus, and stressed/dead cells have disrupted nucleus structure.

One of the major limitations of the proposed assay is the manual segmentation of the signal from a 2D compressed image. Automated segmentation of mitochondrial signals is required for developing a high throughput assay. Specifically, quantifying ROS and mitochondrial cell in apoptotic cells remains challenging since they are detached from the plate and undergo a plane shift. Another limitation of the proposed assay is that it could not monitor cytosolic calcium, mitochondrial calcium overload, and DNA condensation as dye-dye interaction leads to a significant change in cell morphology.

This study shows the efficiency of the FDA-approved drug nifedipine in protecting A549 cells. Although the proof of concept is established with a chemical hypoxia model using $CoCl_2$, further study in an animal model with lung injury is required where the effect of hypoxia, pro-inflammatory effects, and protective effect of nifedipine should be investigated. Testing of nifedipine was performed in monolayer culture of A549 cells, but no data is available to protect against lung injury with ARDS and biodistribution of the drugs in various organs.

A very rare but known adverse effect of nifedipine is drug-induced liver injury, which has been described before [53]. However, in a rabbit model, it has been shown that pre-treatment with nifedipine partially prevented the hypoxia and the inflammation-induced decrease in liver cytochrome P450, thereby reducing hepatic injury [21]. In another study based on human and rat islet culture, it has been shown that prior blocking of Ca^{2+} inflow using nifedipine associates with a reduction in hypoxia-induced damage [29]. Moreover, animal model results indicated that nifedipine and is cardioprotective under hypoxic conditions [20]. Although these results support the fact that nifedipine can reduce hypoxia damage in other tissues outside the cells, a detailed dose-response study in animal models towards severe ARDS will widen the clinical relevance. These will be useful to examine the drug efficacy in the context of tissue-level protection. The proposed protocol can also be used as an assay for further screening of other drugs, including CCBs and GPCR targeting drugs to protect the cells under hypoxia.

Currently, there is no registered trial with nifedipine with COVID-19 patients, and hence nifedipine can be further tested in a clinical trial to check if it plays a role in improving mortality and reducing the risk for intubation and ventilation in patients hospitalized for COVID-19. The

inhaled route has been proposed for nifedipine before for asthma [54], and it is possible that early use of CCBs through the nebulized route may reduce hypoxic injury to alveolar epithelial cells if used as soon a patient is diagnosed with the disease in question (e.g., COVID-19). This can be a potential question to be studied in the clinical trial. Furthermore, Nifedipine lowers systemic blood pressure and therefore can potentially reduce blood pressure in a patient who is already dehydrated by increased respiratory effort – This effect may mitigate the systemic use of nifedipine in the context of viral pneumonia. Another disadvantage of the systemic use of nifedipine is that it may increase the ventilation-perfusion mismatch resulting in reduced arterial oxygen tension [28]. Therefore, the above-mentioned inhaled route may be of use in order to thoroughly examine the clinical benefit of nifedipine in this context. In conclusion, nifedipine treatment can be protective to lung epithelial cells during hypoxia by lowering calcium efflux, mitochondrial load, and ROS generation.

Declaration of competing interest

The authors declare no conflict of interest.

Acknowledgments

The authors acknowledge the research facilities provided by the Indian Institute of Technology Hyderabad, India, and Department of Science and Technology for the fellowship of Kuruba Manohar, and Ministry of Education for the fellowship support for Parth Gupta. We also thank Vaibhav Dhyani, Shibu Chameettachal and Jagadeesh Mahadevan for their suggestions during RT-PCR and IF experiments. This study was supported by the Department of Biotechnology, Ministry of Science & Technology, India (Grant number: BT/PR21261/MED/31/348/2016 and BT/PR22239/NNT/28/1269/2017).

Appendix A. Supplementary data

Supplementary data to this article can be found online at https://doi.org/10.1016/j.freeradbiomed.2021.08.245.

Funding

Department of Biotechnology, Ministry of Science and Technology, Grant/Award Number: BT/PR21261/MED/31/348/2016 and BT/PR22239/NNT/28/1269/2017.

Author contributions

Idea conceptualization: K.M., R.K.G., and G.L.; methodology: K.M., R.K.G., and G.L.; software application: K.M., and G.P.; formal analysis: K.M., G.P., and G.S.; investigation: K.M., R.K.G., G.P., S.R., M.A., and G.L.; resources: M.A., G.L.; data curation: K.M., and G.P.; writing—the original draft of the manuscript: K.M.; reviewing and editing the manuscript: K.M., R.K.G., G.P., S.D., S.R., M.A., and G.L.; data visualization: K.M., G.P., M.A., and G.S; supervision: R.K.G., and M.A., and G.L.; project administration: G.L.; funding acquisition: G.L. All authors read and agreed to the published version of the manuscript.

References

[1] D. Wang, B. Hu, C. Hu, F. Zhu, X. Liu, J. Zhang, B. Wang, H. Xiang, Z. Cheng, Y. Xiong, Y. Zhao, Y. Li, X. Wang, Z. Peng, Clinical characteristics of 138 hospitalized patients with 2019 novel coronavirus-infected pneumonia in Wuhan, China, JAMA, J. Am. Med. Assoc. 323 (2020) 1061–1069, https://doi.org/10.1001/jama.2020.1585.

[2] V. Kryvenko, I. Vadász, Molecular mechanisms of Na,K-ATPase dysregulation driving alveolar epithelial barrier failure in severe COVID-19, Am. J. Physiol. Cell. Mol. Physiol. (2021), https://doi.org/10.1152/ajplung.00056.2021.

[3] M.F. Osuchowski, M.S. Winkler, T. Skirecki, S. Cajander, M. Shankar-Hari, G. Lachmann, G. Monneret, F. Venet, M. Bauer, F.M. Brunkhorst, S. Weis, A. Garcia-Salido, M. Kox, J.-M. Cavaillon, F. Uhle, M.A. Weigand, S.B. Flohé, W. J. Wiersinga, R. Almansa, A. de la Fuente, I. Martin-Loeches, C. Meisel, T. Spinetti, J.C. Schefold, C. Cilloniz, A. Torres, E.J. Giamarellos-Bourboulis, R. Ferrer, M. Girardis, A. Cossarizza, M.G. Netea, T. van der Poll, J.F. Bermejo-Martín, I. Rubio, The COVID-19 puzzle: deciphering pathophysiology and phenotypes of a new disease entity, Lancet Respir. Med. 9 (2021) 622–642, https://doi.org/10.1016/s2213-2600(21)00218-6.

[4] S. Tian, W. Hu, L. Niu, H. Liu, H. Xu, S.Y. Xiao, Pulmonary pathology of early-phase 2019 novel coronavirus (COVID-19) pneumonia in two patients with lung cancer, J. Thorac. Oncol. 15 (2020) 700–704, https://doi.org/10.1016/j.jtho.2020.02.010.

[5] J.H. Sim, M.-H. Choi, H.-J. Shin, J.-E. Lee, Wheatgrass extract ameliorates hypoxia-induced mucin gene expression in A549 cells, pharmacogn, What Mag. 13 (2017) 7–12, https://doi.org/10.4103/0973-1296.197660.

[6] J. Muñoz-Sánchez, M.E. Chánez-Cárdenas, The use of cobalt chloride as a chemical hypoxia model, J. Appl. Toxicol. 39 (2019) 556–570, https://doi.org/10.1002/jat.3749.

[7] Q. Guo, F. Lan, X. Yan, Z. Xiao, Y. Wu, Q. Zhang, Hypoxia exposure induced cisplatin resistance partially via activating p53 and hypoxia inducible factor-1α in non-small cell lung cancer A549 cells, Oncol. Lett. 16 (2018) 801–808, https://doi.org/10.3892/ol.2018.8767.

[8] J. Sim, M.H. Choi, H.J. Shin, J.E. Lee, Wheatgrass extract ameliorates hypoxia-induced mucin gene expression in A549 cells, Pharmacogn, What Mag. 13 (2017) 7–12, https://doi.org/10.4103/0973-1296.197660.

[9] D.M.A. El-ella, Accepted manuscript (unedited) autophagy/apoptosis induced by geraniol through HIF- 1α/BNIP3/beclin -1 signaling pathway in A549 CoCl 2 treated cells accepted manuscript (unedited), (n.d.) 1–16.

[10] W.-C. Chen, M.D. To, P.M.K. Westcott, R. Delrosario, I.-J. Kim, M. Philips, Q. Tran, N. Bayani, A. Balmain, Regulation of KRAS4A/B splicing in cancer stem cells by the RBM39 splicing complex, BioRxiv (2019), https://doi.org/10.1101/646125.

[11] P.J. Kallio, I. Pongratz, K. Gradin, J. McGuire, L. Poellinger, Activation of hypoxia-inducible factor 1α: posttranscriptional regulation and conformational change by recruitment of the Arnt transcription factor, Proc. Natl. Acad. Sci. U.S.A. 94 (1997) 5667–5672, https://doi.org/10.1073/pnas.94.11.5667.

[12] C. Hypoxia, P.S. Cells, neuregulin-1 protects neuronal cells against damage due to 23 (2019) 111–118.

[13] P. Buachan, M. Namsa-aid, W. Tanechpongtamb, Terrein inhibits aggressive phenotype of A549 human lung cancer cell through suppression of HIF, 1α 18 (2021) 1–11.

[14] Y. Fujioka, S. Nishide, T. Ose, T. Suzuki, I. Kato, H. Fukuhara, M. Fujioka, K. Horiuchi, A.O. Satoh, P. Nepal, S. Kashiwagi, J. Wang, M. Horiguchi, Y. Sato, S. Paudel, A. Nanbo, T. Miyazaki, H. Hasegawa, K. Maenaka, Y. Ohba, A sialylated voltage-dependent Ca 2+ channel binds hemagglutinin and mediates influenza A virus entry into mammalian cells, Cell Host Microbe 23 (2018) 809–818, https://doi.org/10.1016/j.chom.2018.04.015, e5.

[15] S.M. Anil, N. Shalev, A.C. Vinayaka, S. Nadarajan, D. Namdar, E. Belausov, I. Shoval, K.A. Mani, G. Mechrez, H. Koltai, Cannabis compounds exhibit anti-inflammatory activity in vitro in COVID-19-related inflammation in lung epithelial cells and pro-inflammatory activity in macrophages, Sci. Rep. 11 (2021) 1–14, https://doi.org/10.1038/s41598-021-81049-2.

[16] E.J. Murphy, C. Masterson, E. Rezoagli, D. O'Toole, I. Major, G.D. Stack, M. Lynch, J.G. Laffey, N.J. Rowan, β-Glucan extracts from the same edible shiitake mushroom Lentinus edodes produce differential in-vitro immunomodulatory and pulmonary cytoprotective effects — implications for coronavirus disease (COVID-19) immunotherapies, Sci. Total Environ. 732 (2020) 139330, https://doi.org/10.1016/j.scitotenv.2020.139330.

[17] X. Chen, R. Cao, W. Zhong, Host calcium channels and pumps in viral infections, Cells 9 (2019) 1–13, https://doi.org/10.3390/cells9010094.

[18] C.L. He, L.Y. Huang, K. Wang, C.J. Gu, J. Hu, G.J. Zhang, W. Xu, Y.H. Xie, N. Tang, A.L. Huang, Identification of bis-benzylisoquinoline alkaloids as SARS-CoV-2 entry inhibitors from a library of natural products, Signal Transduct. Target, Ther 6 (2021) 1–40, https://doi.org/10.1038/s41392-021-00531-5.

[19] B. Chovancova, V. Liskova, S. Miklikova, S. Hudecova, P. Babula, A. Penesova, A. Sevcikova, E. Durinikova, M. Novakova, M. Matuskova, O. Krizanova, Calcium signaling affects migration and proliferation differently in individual cancer cells due to nifedipine treatment, Biochem. Pharmacol. 171 (2020) 113695, https://doi.org/10.1016/j.bcp.2019.113695.

[20] A. Verkhratsky, Calcium and cell death, Subcell. Biochem. 45 (2007) 465–480, https://doi.org/10.1007/978-1-4020-6191-2_17.

[21] D.B. Fitzpatrick, M. Karmazyn, Comparative effects of calcium channel blocking agents and varying extracellular calcium concentration on hypoxia/reoxygenation and ischemia/reperfusion-induced cardiac injury, J. Pharmacol. Exp. Therapeut. 228 (1984) 761. LP – 768, http://jpet.aspetjournals.org/content/228/3/761.abstract.

[22] C.Q. Song, D.Z. Sun, Y.M. Xu, C. Yang, Q. Cai, X.S. Dong, Effect of endoplasmic reticulum calcium on paraquat-induced apoptosis of human lung type II alveolar epithelial A549 cells, Mol. Med. Rep. 20 (2019) 2419–2425, https://doi.org/10.3892/mmr.2019.10469.

[23] S. Yadav, N. Kalra, L. Ganju, M. Singh, Activator protein-1 (AP-1): a bridge between life and death in lung epithelial (A549) cells under hypoxia, Mol. Cell. Biochem. 436 (2017) 99–110, https://doi.org/10.1007/s11010-017-3082-1.

[24] M. Dai, P. Cui, M. Yu, J. Han, H. Li, R. Xiu, Melatonin modulates the expression of VEGF and HIF-1α induced by CoCl2 in cultured cancer cells, J. Pineal Res. 44 (2008) 121–126, https://doi.org/10.1111/j.1600-079X.2007.00498.x.

[25] M.R. Straus, M. Bidon, T. Tang, G.R. Whittaker, S. Daniel, FDA approved calcium channel blockers inhibit SARS-CoV-2 infectivity in epithelial lung cells, BioRxiv (2020) 1–19, https://doi.org/10.1101/2020.07.21.214577.

[26] E. Kwon, H. Yang, Y. Kim, Virus Infection by Suppressing Intracellular Calcium, 2021.
[27] P. Agostoni, E. Doria, G. Galli, G. Tamborini, M.D. Guazzi, Nifedipine reduces pulmonary pressure and vascular tone during short- but not long-term treatment of pulmonary hypertension in patients with chronic obstructive pulmonary disease, Am. Rev. Respir. Dis. 139 (1989) 120–125, https://doi.org/10.1164/ajrccm/139.1.120.
[28] A. Davidson, A. Bossuyt, I. Dab, Acute effects of oxygen, nifedipine, and diltiazem in patients with cystic fibrosis and mild pulmonary hypertension, Pediatr. Pulmonol. 6 (1989) 53–59, https://doi.org/10.1002/ppul.1950060113.
[29] Z. Ma, N. Moruzzi, S.B. Catrina, I. Hals, J. Oberholzer, V. Grill, A. Björklund, Preconditioning with associated blocking of Ca2+ inflow alleviates hypoxia-induced damage to pancreatic β-cells, PLoS One 8 (2013), https://doi.org/10.1371/journal.pone.0067498.
[30] C. Lisk, J. McCord, S. Bose, T. Sullivan, Z. Loomis, E. Nozik-Grayck, T. Schroeder, K. Hamilton, D.C. Irwin, Nrf2 activation: a potential strategy for the prevention of acute mountain sickness, Free Radic. Biol. Med. 63 (2013) 264–273, https://doi.org/10.1016/j.freeradbiomed.2013.05.024.
[31] J. Yao, H. Long, J. Zhao, G. Zhong, J. Li, Nifedipine inhibits oxidative stress and ameliorates osteoarthritis by activating the nuclear factor erythroid-2-related factor 2 pathway, Life Sci. 253 (2020) 117292, https://doi.org/10.1016/j.lfs.2020.117292.
[32] M.J. Jou, Melatonin preserves the transient mitochondrial permeability transition for protection during mitochondrial Ca2+ stress in astrocyte, J. Pineal Res. 50 (2011) 427–435, https://doi.org/10.1111/j.1600-079X.2011.00861.x.
[33] T.C. Sun, X.C. Liu, S.H. Yang, L.L. Song, S.J. Zhou, S.L. Deng, L. Tian, L.Y. Cheng, Melatonin inhibits oxidative stress and apoptosis in cryopreserved ovarian tissues via Nrf2/HO-1 signaling pathway, Front. Mol. Biosci. 7 (2020) 1–11, https://doi.org/10.3389/fmolb.2020.00163.
[34] S.K.S. Sarada, H.P. Veeramohan, T. Mathew, S. Saumya, M. Chitharanjan, Nifedipine inhibits hypoxia induced transvascular leakage through down regulation of NFkB, Respir. Physiol. Neurobiol. 183 (2012) 26–34, https://doi.org/10.1016/j.resp.2012.05.016.
[35] M. Barakat, P. Du Souich, Effect of nifedipine on the elimination of theophylline in the rabbit subjected to hypoxia or to an inflammatory reaction, J. Pharm. Pharmacol. 48 (1996) 906–910, https://doi.org/10.1111/j.2042-7158.1996.tb05999.x.
[36] J.R. Lee, J.Y. Lee, H.J. Kim, M.J. Hahn, J.S. Kang, H. Cho, The inhibition of chloride intracellular channel 1 enhances Ca2+ and reactive oxygen species signaling in A549 human lung cancer cells, Exp. Mol. Med. 51 (2019), https://doi.org/10.1038/s12276-019-0279-2.
[37] P. Bärtsch, E.R. Swenson, Acute high-altitude illnesses, N. Engl. J. Med. 368 (2013) 2294–2302, https://doi.org/10.1056/nejmcp1214870.
[38] M. Akao, B. O'Rourke, Y. Teshima, J. Seharaseyon, E. Marbán, Mechanistically distinct steps in the mitochondrial death pathway triggered by oxidative stress in cardiac myocytes, Circ. Res. 92 (2003) 186–194, https://doi.org/10.1161/01.RES.0000051861.21316.E9.
[39] K.J. Livak, T.D. Schmittgen, Analysis of relative gene expression data using real-time quantitative PCR and the 2-ΔΔCT method, Methods 25 (2001) 402–408, https://doi.org/10.1006/meth.2001.1262.
[40] T. Vicar, M. Raudenska, J. Gumulec, J. Balvan, The quantitative-phase dynamics of apoptosis and lytic cell death, Sci. Rep. 10 (2020) 1–12, https://doi.org/10.1038/s41598-020-58474-w.
[41] M. Ke, Q. Tang, Z. Pan, Y. Yin, L. Zhang, K. Wen, Sphingosine-1-phosphate attenuates hypoxia/reoxygenation-induced cardiomyocyte injury via a mitochondrial pathway, Biochem. Biophys. Res. Commun. 510 (2019) 142–148, https://doi.org/10.1016/j.bbrc.2019.01.067.
[42] L. Zhang, F. Li, X. Su, Y. Li, Y. Wang, R. Fang, Y. Guo, T. Jin, H. Shan, X. Zhao, R. Yang, H. Shan, H. Liang, Melatonin prevents lung injury by regulating apelin 13 to improve mitochondrial dysfunction, Exp. Mol. Med. 51 (2019), https://doi.org/10.1038/s12276-019-0273-8.
[43] M. Lazzeri, A. Lanza, R. Bellini, A. Bellofiore, S. Cecchetto, A. Colombo, F. D'Abrosca, C. Del Monaco, G. Gaudiello, M. Paneroni, E. Privitera, M. Retucci, V. Rossi, M. Santambrogio, M. Sommariva, P. Frigerio, Respiratory physiotherapy in patients with COVID-19 infection in acute setting: a position paper of the Italian association of respiratory physiotherapists (ARIR), Monaldi Arch. Chest Dis. 90 (2020) 163–168, https://doi.org/10.4081/monaldi.2020.1285.
[44] R.B.N. Or Caspi, Michael J. Smart, Since January 2020 Elsevier has created a COVID-19 resource centre with free information in English and Mandarin on the novel coronavirus COVID-, Ann. Oncol. (2020) 19–21.
[45] Y. Liu, J. Lv, J. Liu, M. Li, J. Xie, Q. Lv, W. Deng, N. Zhou, Y. Zhou, J. Song, P. Wang, C. Qin, W.M. Tong, B. Huang, Mucus production stimulated by IFN-AhR signaling triggers hypoxia of COVID-19, Cell Res. 30 (2020) 1078–1087, https://doi.org/10.1038/s41422-020-00435-z.
[46] Z.O. Serebrovska, E.Y. Chong, T.V. Serebrovska, L.V. Tumanovska, L. Xi, Hypoxia, HIF-1α, and COVID-19: from pathogenic factors to potential therapeutic targets, Acta Pharmacol. Sin. 41 (2020) 1539–1546, https://doi.org/10.1038/s41401-020-00554-8.
[47] A.L. Lai, J.K. Millet, S. Daniel, J.H. Freed, G.R. Whittaker, Since January 2020 Elsevier Has Created a COVID-19 Resource Centre with Free Information in English and Mandarin on the Novel Coronavirus COVID- Company ' S Public News and Information Website, Elsevier hereby grants permission to make all its COVID-19-r, 2020.
[48] T. Tang, M. Bidon, J.A. Jaimes, G.R. Whittaker, S. Daniel, Since January 2020 Elsevier Has Created a COVID-19 Resource Centre with Free Information in English and Mandarin on the Novel Coronavirus COVID- 19 . The COVID-19 Resource Centre Is Hosted, Elsevier Connect the company ' s public news and information, 2020.
[49] Y. Xu, C. Duan, Z. Kuang, Y. Hao, J.L. Jeffries, G.W. Lau, Pseudomonas aeruginosa pyocyanin activates NRF2-ARE-mediated transcriptional response via the ROS-EGFR-PI3K-AKT/MEK-ERK MAP kinase signaling in pulmonary epithelial cells, PLoS One 8 (2013) 1–13, https://doi.org/10.1371/journal.pone.0072528.
[50] A. Kobayashi, M.-I. Kang, H. Okawa, M. Ohtsuji, Y. Zenke, T. Chiba, K. Igarashi, M. Yamamoto, Oxidative stress sensor Keap1 functions as an adaptor for cul3-based E3 ligase to regulate proteasomal degradation of Nrf2, Mol. Cell Biol. 24 (2004) 7130–7139, https://doi.org/10.1128/mcb.24.16.7130-7139.2004.
[51] K. Itoh, T. Chiba, S. Takahashi, T. Ishii, K. Igarashi, Y. Katoh, T. Oyake, N. Hayashi, K. Satoh, I. Hatayama, M. Yamamoto, Y. ichi Nabeshima, An Nrf2/small Maf heterodimer mediates the induction of phase II detoxifying enzyme genes through antioxidant response elements, Biochem. Biophys. Res. Commun. 236 (1997) 313–322, https://doi.org/10.1006/bbrc.1997.6943.
[52] D. Caldeira, J. Alarcão, A. Vaz-Carneiro, J. Costa, Risk of pneumonia associated with use of angiotensin converting enzyme inhibitors and angiotensin receptor blockers: systematic review and meta-analysis, BMJ 345 (2012) 2020–2022, https://doi.org/10.1136/bmj.e4260.
[53] D. Yusuf, J. Christy, D. Owen, M. Ho, D. Li, M.J. Fishman, A case report of nifedipine-induced hepatitis with jaundice, BMC Res. Notes 11 (2018) 1–9, https://doi.org/10.1186/s13104-018-3322-9.
[54] A. Knox, A. Tattersfield, J.R. Britton, The effect of inhaled ouabain on bronchial reactivity to histamine in man, Br. J. Clin. Pharmacol. 25 (1988) 758–760, https://doi.org/10.1111/j.1365-2125.1988.tb05264.x.
[55] I Uzieliene, E Bernotiene, G Rakauskiene, J Denkovskij, E Bagdonas, Z Mackiewicz, N Porvaneckas, G Kvederas, A Mobasheri, The antihypertensive drug nifedipine modulates the metabolism of chondrocytes and human bone marrow-derived mesenchymal stem cells, Front. Endocrinol. (2019), https://doi.org/10.3389/fendo.2019.00756.